Potential Energy Surfaces for Rearrangements of Berson Trimethylenemethanes

ARTICLE *in* THE JOURNAL OF PHYSICAL CHEMISTRY A · MARCH 2012

Impact Factor: 2.69 · DOI: 10.1021/jp211518f · Source: PubMed

2 AUTHORS:

Uğur Bozkaya
Hacettepe University
32 PUBLICATIONS **331** CITATIONS
SEE PROFILE

Ilker Ozkan
Middle East Technical University
1 PUBLICATION **13** CITATIONS
SEE PROFILE

THE JOURNAL OF PHYSICAL CHEMISTRY A

Article

pubs.acs.org/JPCA

Potential Energy Surfaces for Rearrangements of Berson Trimethylenemethanes

Uğur Bozkaya*,†,‡ and İlker Özkan*,‡

†Department of Chemistry, Atatürk University, Erzurum 25240, Turkey

‡Department of Chemistry, Middle East Technical University, Ankara 06800, Turkey

Supporting Information

ABSTRACT: In this research, thermal rearrangements of the Berson trimethylenemethanes (Berson-TMMs) have been investigated by employing density functional theory (DFT) and high-level ab initio methods, such as the complete active space self-consistent field (CASSCF), multireference second-order Møller–Plesset perturbation theory (MRMP2), multireference configuration interaction singles and doubles (MRCISD), and coupled-cluster singles and doubles with perturbative triples [CCSD(T)]. In all computations Pople's polarized triple-ζ split valence basis set, 6-311G(d,p), is utilized. The relevant portions of the lowest-energy, singlet-spin potential energy surface of the C_4H_6 (parent TMM), C_6H_8 (Berson-TMMa), and C_8H_{12} (Berson-TMMc) chemical systems have been explored in order to determine the reaction energies and activation parameters accurately, with the ultimate objective of providing a theoretical account of experiments by Berson on TMMc. The nature of the orthogonal and the planar structures of the parent TMM have been clarified in this study. We have concluded that the orthogonal TMM $^1B_1$ minimum has a C_{2v} symmetry structure, and there is no pyramidalization in the unique methylene group. It lies at 13.9 kcal mol^{-1} above the triplet minimum $^3B_2$ at MRCISD level. The closed-shell $^1A_1$ state of the planar TMM is not a true minimum but a transition structure (TS) for 180° rotation of the unique methylene group in the orthogonal TMM minimum. It lies at 3.0 kcal mol^{-1} above $^1B_1$. The planar structures are also involved in the interchange of equivalent orthogonal TMMs ($\mathbf{o}_1$, $\mathbf{o}_2$, $\mathbf{o}_3$). Many features of the parent TMM are retained in TMMa and TMMc, despite the constraints imposed by the five-membered ring in the latter species. Thus, ring closure to the bicyclic molecules **3a** (**3c**) and **5a** (**5c**) takes place similarly to that in the parent TMM. Likewise, planar TMMa (TMMc) structures are TSs, while orthogonal ones are true minima. The adiabatic singlet–triplet gaps are also similar, being 14.7 (13.0) and 16.5 (16.2) kcal mol^{-1} in the orthogonal ($\mathbf{o}_1$) and planar TMMa (TMMc), respectively. It has been shown here that the substantial reductions in the ring-opening barriers of MCP derivatives **3a** (**3c**) and **5a** (**5c**) can be largely attributed to ring strain in the former and π-bond strain in the latter species.

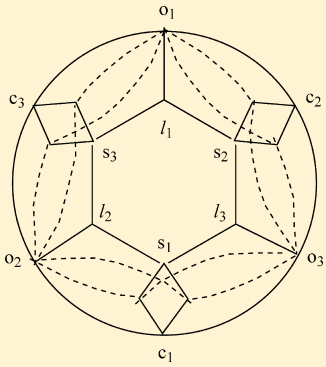

INTRODUCTION

It is rare in hydrocarbon chemistry to encounter intermediates that are kinetically stable and yet cannot be represented by classical resonance structures due to their lacking at least one bond from the number predicted by standard rules of valence. Because of this they are called non-Kekulé molecules.[1−4] Reactive intermediates arising from substituted methylenecyclopropanes (MCPs) are such molecules, often referred to as trimethylenemethanes (TMMs).[5−9] The bonding pattern of TMM is shown in Figure 1.

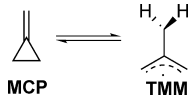

Figure 1. Ring-opening reaction of MCP leading to (orthogonal) TMM.

TMM is one of the most popular organic intermediates that has been studied both experimentally[10−22] and theoretically.[23−48] Experimental identification of TMM from the photolysis of 4-methylene-1-pyrazoline was reported by Dowd[10] in 1966. The electron spin resonance (ESR) spectrum of TMM indicated that the ground state of TMM is triplet. The confirmation of the triplet ground state was accomplished in 1976.[11]

A number of experimental studies were carried out in order to investigate methylenecyclopropane degenerate rearrangements.[4] MCP is surprisingly stable upon heating. However, at temperatures above 150 °C, substituted MCPs exhibit a degenerate isomerization that interchanges ring and exo-methylene carbons, a reaction that appears to involve the trimethylenemethane (TMM) biradical. In 1963, Chesick[49] measured the activation energy for the reversible isomerization of 2-methyl-MCP to ethylidenecyclopropane (Figure 2) as 40.4 kcal mol^{-1}. In a 1986 study, LeFevre and Crawford[50] determined that the activation energy and enthalpy for the isomerization of dideuteriomethylenecyclopropane to methyl-

Received: November 30, 2011
Revised: February 7, 2012
Published: February 8, 2012

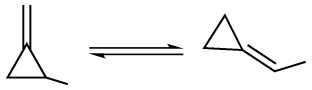

Figure 2. Isomerization of 2-methyl-MCP to ethylidenecyclopropane.

enecyclopropane-2,2-d_2 (Figure 3) are 41.2 ± 0.8 and 40.5 ± 0.8 kcal mol^{-1}, respectively.

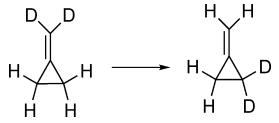

Figure 3. Isomerization of dideuteriomethylenecyclopropane to methylenecyclopropane-2,2-d_2.

The simple Hückel method predicts a triplet ground state for TMM as long as its electronic structure is characterized by two degenerate frontier molecular orbitals (FMO's) (Figure 4). For

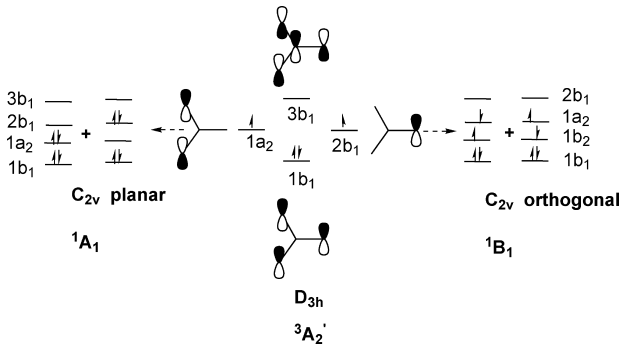

Figure 4. The π-system of TMM and the electronic configurations of the three lowest states. C_{2v} labels are used at the ground state equilibrium geometry (D_{3h}) of the triplet state, where the $1a_2$ and $2b_1$ orbitals are two degenerate e′ components. Two different distortions can lift the degeneracy between these orbitals (and the two lowest excited states, i.e., $^1A_1$ and $^1B_1$). One is a C_{2v} distortion, which leaves the molecule planar, whereas another involves a 90° rotation of one of the CH_2 groups. The former distortion stabilizes the $1a_2$ orbital and the closed-shell $^1A_1$ singlet state (shown on the left), whereas the latter favors the $2b_1$ orbital and the open-shell $^1B_1$ singlet state (shown on the right). Note that at the orthogonal C_{2v} geometry, the b_1 and b_2 labels interchange.

planar D_{3h} geometry, the ground state of TMM is $^3A'_2$. If one retains planar D_{3h} geometry, but descends to C_{2v}, the ground state will be designated as $^3B_2$. Occupation of the two degenerate orbitals will yield several different singlet states. One of these states is formed by double occupation of one of two degenerate orbitals to create a planar closed-shell singlet, which can be stabilized by a Jahn–Teller[51] distortion. Another is formed by single occupation of the two degenerate orbitals and gives a planar open-shell singlet that can be stabilized by a different Jahn–Teller distortion. Finally, a 90° rotation of one methylene group yields a C_{2v} structure. This situation is summarized in Figure 5.

A great number of theoretical computations have been carried out in order to predict relative energies and to define the nature of each TMM as to whether it is a minimum or a transition state or whatever. Most of early computations[23−39] predicted that both $^1B_1$ and $^1A_1$ states are minima on the potential energy surface, and that the $^1B_1$ state is lower in energy than the $^1A_1$ state. Borden and Davidson[27] estimated that the planar $^1B_2$ state is a transition state for the pseudorotation of the $^1A_1$ state. Furthermore, Davis and Goddard[25] predicted that the $^1B_2$ state is unstable with respect to rotation of one of the methylene units to form a stable, nonplanar $^1B_1$ state. Therefore, the $^1B_2$ state of TMM is a maximum in two coordinates on the potential energy surface (a "mountain top"). The computations of Borden[42] at the (4e,4o)CASSCF/6-31G* level of theory suggest that $^1A_1$ TMM is a saddle point that connects two equivalent C_2 states. Each C_2 state is a transition state that exchanges the out-of-plane methylene with a planar methylene in the $^1B_1$ state. However, the imaginary frequency at this level of theory is only 70i. At the (10e,10o)CASSCF/cc-pVTZ levels of theory, Cramer's computations[39] estimated that the $^1A_1$ state is a minimum, while the $^1B_1$ state is a transition structure. The eigenvector that is associated with the imaginary frequency pyramidalizes the rotated methylene. Cramer was able to find a minimum for the pyramidalized structure. The extent of pyramidalization was small, only 10° away from C_{2v} geometry.

The energy difference between the singlet and triplet states of TMM (the "*singlet–triplet splitting*") has been of considerable interest. Dowd's experiments[13,14] indicated that the energy separation between the lowest singlet and triplet states was 7.8 ± 0.3 kcal mol^{-1}. In that experiment, Dowd measured the temperature dependence of the rate of disappearance of the ESR signal for the matrix isolated triplet biradical. If it is assumed that the rate-determining step for the signal loss is intersystem crossing, then the measured activation energy can be equated with the singlet–triplet splitting. However, early computational studies[23−38] predicted the energy difference between the $^3A'_2$ and $^1B_1$ states to be 15–20 kcal mol^{-1}. Cramer's computations[39] at the (10e,10o)CASPT2N/cc-pVTZ level suggested that the energy difference between the $^3A'_2$ and $^1B_1$ states was 16.1 kcal mol^{-1}, and $^1B_1$ state was 3 kcal mol^{-1} lower in energy than $^1A_1$ state. Thus, Dowd's experiments led to a disagreement between experimental and theoretical results. A number of theoretical studies was carried out to understand the controversy. Davidson[33] pointed out that the experimentally measured value of 7.8 ± 0.3 kcal mol^{-1} may not correspond to singlet–triplet splitting of $^3A'_2$ and $^1B_1$ state. Instead, the disappearance of the ESR signal may be arising

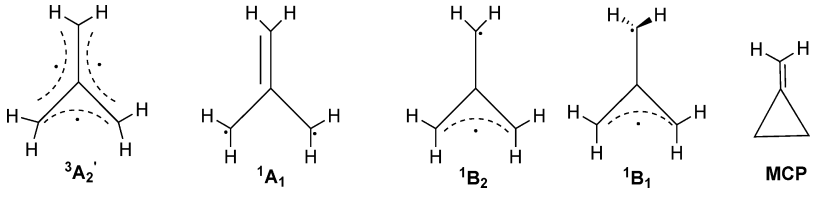

Figure 5. Qualitative structures of TMMs and MCP.

dx.doi.org/10.1021/jp211518f | J. Phys. Chem. A 2012, 116, 2309–2321

from the closure to MCP by crossing of the triplet to the singlet surface.

Photoelectron spectroscopy (PS) of the TMM radical anion has suggested that the $^1A_1$ state lies 16.1 kcal mol^{-1} above the triplet ground state. The $^1B_1$ state was not observed in the photoelectron spectrum due to the fact that the Franck–Condon overlap was insufficient to observe the $^1B_1$ state spectroscopically.[20−22]

Due to their unusual electronic structures, TMM derivatives have been extensively studied both experimentally[2,5−9,32,52−62] and theoretically.[31,46,63,64] In particular, spectroscopic and chemical experiments with monocyclic TMM derivatives by Berson's group at Yale University have been instrumental in raising our understanding of TMMs to a high level.[7−9] The singlet–triplet energy splitting (ΔE_{ST}) of other TMMs have not been experimentally measured. However, thermochemical estimates indicate that the singlet–triplet energy spacing in TMM derivatives does not differ by more than several kcal mol^{-1} from that in the parent TMM.[7]

Berson et al.[55] published their experimental estimation of singlet–triplet energy separation for 2-isopropylidenecyclopenta-1,3-diyl (**1c**) (Figure 6), a TMM derivative, in 1982. They

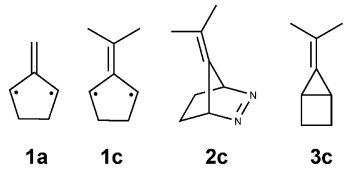

Figure 6. Structures of molecules **1a**, **1c**, **2c**, and **3c**.

suggested that the singlet biradical **1c** was 13.3 kcal mol^{-1} higher in energy than compound **3c**. Since triplet **1c** is more stable than compound **3c** due to the high ring strain in the latter, the singlet–triplet energy separation was estimated as ≥13.3 kcal mol^{-1}, which was in poor agreement with their previously reported experimental value of <3.5 kcal mol^{-1}.[65] Dixon et al.[31] computed that singlet–triplet splitting between $^3B_2$ and $^1B_1$ states of 2-methylenecyclopenta-1,3-diyl (**1a**) is 15.2 kcal mol^{-1} and that the $^1A_1$ state is 6.0 kcal mol^{-1} higher in energy than $^1B_1$ state at (4e,4o)CASSCF/STO-3G level.

Both singlet and triplet **1c** can be generated from azoalkane **2c** via thermal and photochemical denitrogenation, respectively[9,53−57] (Figure 7). The triplet species is readily observed

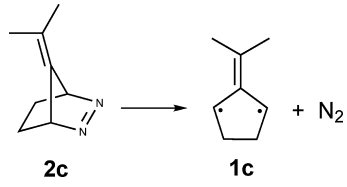

Figure 7. Decomposition of **2c** to **1c**.

by ESR spectroscopy.[57] Its reactions with olefins are stereorandom. In the absence of olefins it dimerizes.[7,9,53,54,56] These observations suggest that the molecule in its triplet state reacts by two successive bond-forming steps. Characterization of the singlet species has been more difficult, since it has no ESR spectrum. Its reactions with olefins appear to be stereospecific, and this suggests an intermediate with singlet-paired electron spins, which in turn gives cycloadducts by forming two bonds in a concerted manner. Structural rearrangements and stereomutations (geometrical isomerizations) of TMMs are usually formulated with the singlet state of **1c** (Figure 8).

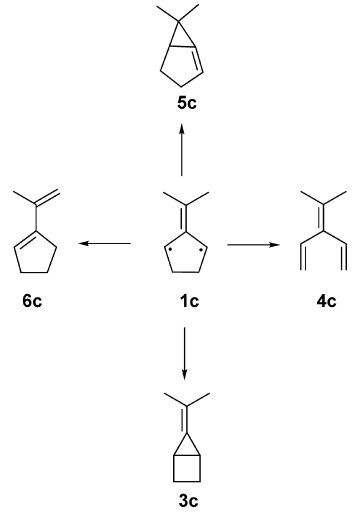

Figure 8. Rearrangements of **1c** to **3c**, **4c**, **5c**, and **6c**.

In this research, a comprehensive theoretical investigation of the thermal rearrangements of Berson-TMMs is carried out by employing the density functional theory (DFT) and high level ab initio methods, such as the complete active space self-consistent field (CASSCF),[66−77] multireference second-order Møller–Plesset perturbation theory (MRMP2),[78−85] multireference configuration interaction singles and doubles (MRCISD),[77,86−88] and coupled-cluster singles and doubles with perturbative triples [CCSD(T)].[89−95] The potential energy surfaces (PESs) for the Berson-TMMs (TMMa and TMMc) are explored to provide a theoretical account of experiments by Berson.[7−9]

■ COMPUTATIONAL METHODS

The computations in this study have mostly been carried out by using the Gaussian 03 (RevD.01) program[96] and the GAMESS package.[97] Gaussian 03 is used for DFT and coupled-cluster (CC) computations, whereas GAMESS is used for the CASSCF,[66−77] MRMP2,[78−85] and MRCISD[77,86−88] computations. For three-dimensional chemical drawings, the CHEMVP program is used.[98]

Geometry optimizations for the closed-shell and high-spin open-shell molecules are performed with the DFT method (B3LYP functional[99,100]). Vibrational frequencies are computed to characterize each stationary structure as a minimum, transition structure (TS), or whatever. After locating a TS, intrinsic reaction coordinate (IRC)[101−105] computations are carried out. In order to improve the computed energies, single-point frozen-core CCSD(T)[89−95] computations are carried out at optimized DFT geometries. In all computations Pople's polarized triple-ζ split valence basis set, 6-311G(d,p), is employed.[106−108] For biradicals, geometry optimization and frequency computations are performed with the CASSCF method. At optimized geometries of these species, single-point MRMP2 computations are carried out to improve the energy values.

In order to obtain a unique energy scale at the CCSD(T)/6-311G(d,p) level for biradicals, vertical singlet–triplet energy differences obtained via MRMP2 computations are used with

dx.doi.org/10.1021/jp211518f | J. Phys. Chem. A 2012, 116, 2309−2321

CCSD(T) energies of the corresponding triplet states to obtain the final energy of singlet biradicals. This approximation can be formalized by

$$E(^1\mathrm{X}) = E_{\mathrm{CCSD(T)}}(^3\mathrm{X}) + E_{\mathrm{MRMP2}}(^1\mathrm{X}) - E_{\mathrm{MRMP2}}(^3\mathrm{X}) \quad (1)$$

where X is a biradical and $E(^1\mathrm{X})$ is the final energy of species $^1\mathrm{X}$.

RESULTS AND DISCUSSION

Thermal Ring-Opening Reaction of Methylenecyclopropane, and the Parent TMM System. Initially, the potential energy surface of parent TMM has been studied. Qualitative structures of TMM and MCP are illustrated in Figure 9. Zero-point vibrational energy (ZPVE) corrected

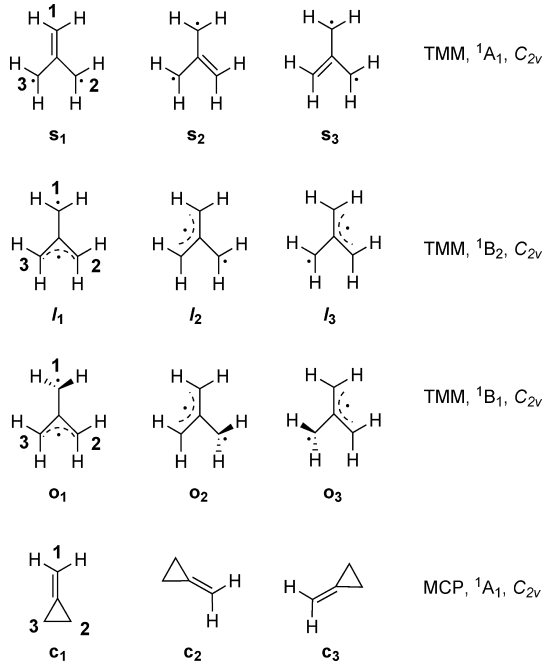

Figure 9. Qualitative structures of TMMs and MCP. Definition of abbreviations: **s**, short planar; **l**, long planar; **o**, orthogonal methylene group; **c**, cyclopropane ring. In all structures, carbon atoms of methylene groups are labeled by 1, 2, and 3 clockwise starting with the top methylene. The subscripts n = 1, 2, and 3 in $\mathbf{s}_n$, $\mathbf{l}_n$, $\mathbf{o}_n$, and $\mathbf{c}_n$ indicate the position of the double bond (i.e., "short" bond), long bond, orthogonal methylene, or cyclopropane ring.

relative energies of parent TMM structures are reported in Table 1 at CASSCF/6-311G(d,p), MRMP2/6-311G(d,p), and MRCISD/6-311G(d,p) levels. For parent TMM structures an active space that consists of four electrons and four orbitals (4e,4o) have been used for the CASSCF and MRMP2 computations. The MRMP2 and MRCISD computations have been carried out at optimized CASSCF geometries. Four electronic states of TMM, namely, $^3A'_2$ ($^3B_2$ in C_{2v} subgroup), $^1A_1$, $^1B_1$, $^1B_2$, and the ground electronic state of MCP have been investigated.

Triplet TMM. With the CASSCF method we have calculated that the triplet TMM is a minimum on the potential energy surface at D_{3h} geometry (state symmetry is $^3A'_2$). In order to construct a relative energy scale for the parent TMMs we use the triplet TMM ($^3A'_2$) as a reference molecule and we set

Table 1. ZPVE Corrected Relative Energies (in kcal mol^{-1}) of the Parent TMM Species, MCP, TS (MCP/o_1), Conrot, and Disrot Structures with 6-311G(d,p) Basis Set

structure	(4e,4o) CASSCF	(4e,4o) MRMP2	(4e,4o) MRCISD[a]	CCSD(T)
triplet	0.0	0.0	0.0	0.0
$\mathbf{o}_1$	13.7	14.9	12.7	
$\mathbf{s}_1$	17.2	18.0	16.9	
$\mathbf{l}_1$	16.7	16.7		
MCP	−13.0	−16.2	−21.2	−22.5
TS (MCP/$\mathbf{o}_1$)	17.2	17.4		
conrot	19.3	20.1		
disrot	18.9	19.6		

[a]Includes Davidson's correction for unlinked quadruple excitations.

relative energy of the triplet to zero. Therefore, energies of other structures will be given relative to the energy of triplet TMM. Further, in order to obtain the relative energy of the MCP we used the RCCSD(T) energy for MCP and UCCSD(T) energy for triplet TMM at optimized CASSCF geometries. Since two π-type active orbitals of TMM will transform to two σ-type orbitals in MCP, the active space will be somewhat modified. In order to obtain reliable energy differences with the CASSCF method the MOs in the active spaces should be similar. Hence, the CASSCF energy differences between TMMs and MCP may not be reliable. On the other hand, we used the CASSCF and MRMP2 energy differences for biradicalic TMM structures, since the RCCSD(T) method suffers from triplet instabilities,[67] while the UCCSD(T) method suffers from high spin contamination for singlet TMMs. The computed geometry of triplet TMM ($^3A'_2$) is shown in Figure 10.

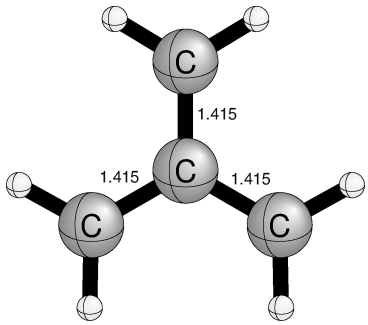

Figure 10. Selected interatomic distances (Å) for the triplet TMM (D_{3h}, $^3A'_2$).

Orthogonal TMM. With the CASSCF method the optimum geometry of the $\mathbf{o}_1(^1B_1)$ structure at C_{2v} symmetry is a transition state with an imaginary frequency of 264i cm^{-1}, connecting two equivalent pyramidalized structures. We found a minimum at C_s geometry with a slightly pyramidalized (12.9°) methylene group that includes the C_1 atom (see Figure 9 for numbering of the TMM carbon atoms). The state symmetry of the C_s structure is A″. However, the $\mathbf{o}_1$(A″) structure is only 0.1 kcal mol^{-1} lower in energy than $\mathbf{o}_1(^1B_1)$ with the CASSCF method, whereas $\mathbf{o}_1(^1B_1)$ is 0.8 kcal mol^{-1} lower in energy than $\mathbf{o}_1$(A″) with MRMP2. Therefore, we conclude that pyramidalization is an artifact of the CASSCF method, and the actual geometry is C_{2v} ($^1B_1$ structure). The relative energy of the o_1 structure is 13.7 and 14.9 kcal mol^{-1} with the CASSCF and MRMP2 methods, respectively. Both the CASSCF and

dx.doi.org/10.1021/jp211518f | J. Phys. Chem. A 2012, 116, 2309−2321

MRMP2 energies are consistent with the Berson's prediction of singlet−triplet splitting energy ≥13.5 kcal mol^{-1} ($\Delta E_{ST} \geq 13.5$ kcal mol^{-1})[7] and also in agreement with Wenthold et al.'s[21,22] estimate of 13−16 kcal mol^{-1}. Further, in order to show that relative energies of the singlet and triplet states of biradicals are reliably computed by the CASSCF and MRMP2 methods, we performed highly expensive MRCISD computations for the parent system. At the MRCISD level the calculated relative energy of $\mathbf{o}_1$ is 12.7 kcal mol^{-1}, which is consistent with both the CASSCF and MRMP2 methods. The computed geometries of $\mathbf{o}_1(^1B_1)$ and $\mathbf{o}_1(^1A'')$ structures are shown in Figure 11.

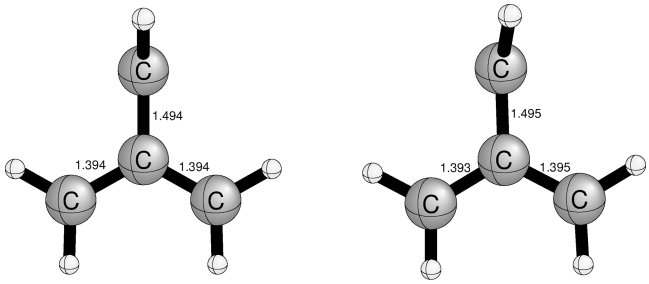

(a) $\mathbf{o}_1$ (C_{2v}, $^1B_1$) (b) $\mathbf{o}_1$ (C_s, $^1A''$)

Figure 11. Selected interatomic distances (Å) for $\mathbf{o}_1(C_{2v},{}^1B_1)$ and $\mathbf{o}_1(C_s,{}^1A'')$ structures.

Planar TMMs. We found that the $\mathbf{l}_1(^1B_2)$ structure is a third-order saddle point at C_{2v} symmetry with the CASSCF method. Corresponding imaginary frequencies are 655i, 378i, and 271i cm^{-1}. The vibrational mode corresponding to imaginary frequency 655i cm^{-1} connects $\mathbf{s}_2$ and $\mathbf{s}_3$ structures by a reaction path which has C_s symmetry. Therefore, this mode will connect $\mathbf{s}_1$ and $\mathbf{s}_3$ structures with $\mathbf{l}_2$, but $\mathbf{s}_1$ and $\mathbf{s}_2$ structures with $\mathbf{l}_3$. The vibrational mode corresponding to imaginary frequency 378.3i connects two equivalent structures with slightly pyramidalized methylene groups by a reaction path which has C_s symmetry. As stated previously for the orthogonal TMM, we conclude that this mode is an artifact of the CASSCF method. The vibrational mode corresponding to imaginary frequency 271.1i yields the orthogonal structure $\mathbf{o}_1$ by a reaction path which has C_2 symmetry. Therefore, this mode will yield the $\mathbf{o}_2$ structure in $\mathbf{l}_2$ and the $\mathbf{o}_3$ structure in $\mathbf{l}_3$. The relative energy of the $\mathbf{l}_1(^1B_2)$ structure is 16.7 kcal mol^{-1} at both the CASSCF and MRMP2 levels. The computed geometries of the $\mathbf{l}_1(^1B_2)$ structure is shown in Figure 12.

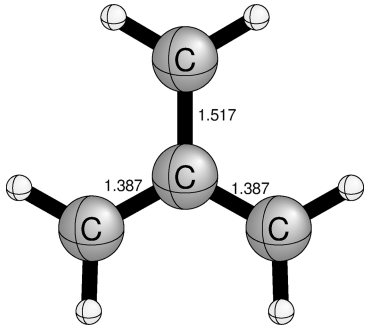

Figure 12. Selected interatomic distances (Å) for the $\mathbf{l}_1(C_{2v},{}^1B_2)$ structure.

We calculated that the $\mathbf{s}_1(^1A_1)$ structure is a minimum on the potential surface at C_{2v} symmetry with the CASSCF method. However, we found a TS for a slightly modified s_1 structure at C_1 symmetry, which has the "same" energy as the $\mathbf{s}_1(^1A_1)$ structure. This transition structure persists with larger basis sets such as cc-pVTZ . Furthermore, we next considered whether the nature of s_1 structure changes with substituents or not. For this purpose, we investigated the methyl TMM (Me-TMM) and Berson-TMMs. For Me-TMM we found only transition structures, and for Berson-TMMa we found both a minimum (at C_2 geometry) and a transition structure (at C_{2v} geometry), but the transition structure was lower in energy than the minimum at the CASSCF and MRMP2 levels, and for Berson-TMMc we found a TS at C_2 geometry. Therefore, we conclude that the potential energy surface around the $\mathbf{s}_1$ structure is very flat and the $^1A_1$ state is a transition state in fact. Relative energy of the $^1A_1$ state is 17.2 and 18.0 kcal mol^{-1} at the CASSCF and MRMP2 levels, respectively. Further, at the MRCISD level the calculated relative energy of the $^1A_1$ state of parent TMM is 16.9 kcal mol^{-1}, which differs by only 0.3 and 1.1 kcal mol^{-1} from the CASSCF and MRMP2 methods, respectively. The computed geometries of $\mathbf{s}_1(^1A_1)$ and $\mathbf{s}_1(^1A)$ structures are shown in Figure 13.

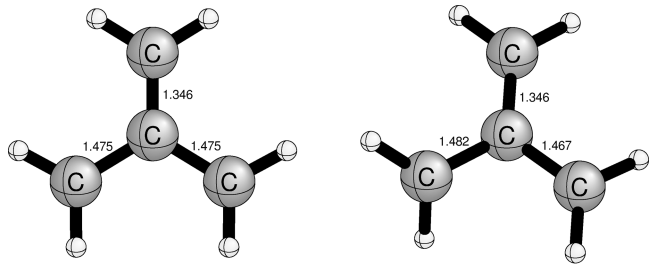

(a) $\mathbf{s}_1$ (C_{2v}, $^1A_1$) (b) $\mathbf{s}_1$ (C_1, ^1A)

Figure 13. Selected interatomic distances (Å) for the $s_1(C_{2v},{}^1A_1)$ and $s_1(C_1,{}^1A)$ structures.

Wenthold et al. measured the energy difference between the $^1A_1$ and $^3A'_2$ states as 16.1 ± 0.2 kcal mol^{-1} and the enthalpy of formation for the triplet TMM as 70 ± 3 kcal mol^{-1}. Further, they estimated the energy difference between the $^1B_1$ and $^3A'_2$ states to be 13−16 kcal mol^{-1}.[21,22] However, observing the $^1A_1$ state by photoelectron spectroscopy does not demonstrate that the $^1A_1$ state is a minimum. With negative ion photoelectron spectroscopy it is possible to study transition states.[21,22] In the system under interest, an electron can be used to "lock" the geometry of the anion close to that of a neutral transition state. With vertical photodetachment the neutral transition state can be generated, and spectroscopic information on that transition state can be obtained directly from the analysis of photoelectron spectrum.[109] In principle, this approach is very close to that used by Zewail et al.[110] Since the geometry of the TMM anion may be close to that of the $^1A_1$ state, it is possible to observe the $^1A_1$ transition state by photoelectron spectroscopy.[21,22] Furthermore, Wenthold et al.[21,22] stated that "*if the* $^1A_1$ *state is a transition state, it must be in a region of the potential energy surface that is exceptionally flat*". Thus, this interpretation is also consistent with our computational observations.

The $\mathbf{s}_1$ structure is 0.5 and 1.3 kcal mol^{-1} higher in energy than the $\mathbf{l}_1$ structure at CASSCF and MRMP2 levels, respectively. However, it is expected that the long planar structure ($\mathbf{l}_1$) would be higher in energy than the short planar

dx.doi.org/10.1021/jp211518f | J. Phys. Chem. A 2012, 116, 2309−2321

structure ($\mathbf{s}_1$). Since, the $\mathbf{s}_1$ structure is a minimum, while $\mathbf{l}_1$ is a third-order saddle point at the CASSCF level, the ZPVE of $\mathbf{l}_1$, 49.3 kcal mol^{-1}, is 1.0 kcal mol^{-1} lower than that of $\mathbf{s}_1$, 50.3 kcal mol^{-1}. Hence, if one only considers the electronic energy differences, the relative energy of $\mathbf{l}_1$ is 19.7, whereas the relative energy of $\mathbf{s}_1$ is 19.4 kcal mol^{-1} at the CASSCF level. Thus, without including ZPVEs, the electronic energy differences are consistent with our expectation. Furthermore, this result also points out that the real natures of the $\mathbf{s}_1$ and $\mathbf{l}_1$ structures are not reflected by the CASSCF method.

Methylenecyclopropane. The MCP structure is a minimum on the potential surface at C_{2v} geometry with the CASSCF method. Relative energy of MCP is −13.0, −16.2, and −22.5 kcal mol^{-1} at the CASSCF, MRMP2, and CCSD(T) levels, respectively. The experimental value for heat of formation of MCP is 47.9 ± 0.4 kcal mol^{-1},[39] while for triplet TMM it is 70 ± 3 kcal mol^{-1}.[21,22] Thus, the experimental energy of MCP relative to triplet TMM is −22.1 kcal mol^{-1}. At the CASSCF level, the computed relative energy of −13.0 kcal mol^{-1} is in poor agreement with the experiment. This result confirms our expectation that the CASSCF energy difference between MCP and triplet TMM is not reliable due to the qualitatively different active spaces. The MRMP2 method somewhat compensates the inconsistencies arising from the different active spaces and yields a relative energy of −16.2 kcal mol^{-1} for MCP. But, the MRMP2 relative energy is in error by 5.9 kcal mol^{-1}, which is still not in good agreement with the experiment. However, the CCSD(T) relative energy of −22.5 kcal mol^{-1} is in very good agreement with the experimental value of −22.1 kcal mol^{-1}. Further, at the MRCISD level the calculated relative energy of MCP is −21.2 kcal mol^{-1}, which differs by 8.2 and 5.0 kcal mol^{-1} from the CASSCF and MRMP2 methods, respectively, while differing by only 0.4 kcal mol^{-1} from the CCSD(T) results. Consequently, these observations verify our expectation that the CCSD(T) relative energy is more reliable than those of the CASSCF and MRMP2 methods for MCP.

Ring-Opening Reaction of Methylenecyclopropane. The relative energy of the transition state that corresponds to ring-opening of MCP is computed as 17.2 and 17.4 kcal mol^{-1} at the CASSCF and MRMP2 levels, respectively. The transition structure forms by an initial cleavage of the C_2−C_3 bond in MCP ($\mathbf{c}_1$) followed by a 90° rotation of only one of the ring methylene groups, in agreement with a suggestion first made by Gajewski,[111,112] and connects MCP to the orthogonal TMM (Figure 14). The activation energy for ring-opening of MCP is

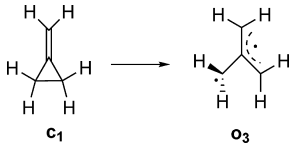

Figure 14. Ring-opening reaction of methylenecyclopropane.

computed to be 39.9 kcal mol^{-1} (relative energy of TS at MRMP2 level minus relative energy of MCP at CCSD(T) level, $E_{TS[mrmp2]} - E_{MCP[ccsd(t)]}$). It is in good agreement with the experimental value of 41.2 ± 0.8 kcal mol^{-1}.[50] Further, we found that the structures corresponding to conrotatory (conrot) and disrotatory (disrot) ring-openings of MCP[33] are mountain tops. Each structure connects MCP to $\mathbf{s}_1$ via a vibrational mode corresponding to one of the two imaginary frequencies, while it connects MCP to $\mathbf{o}_1$ via the vibrational mode corresponding to the other imaginary frequency. The mountain tops have C_2 and C_s geometries, respectively. Relative energy of the conrot structure is 19.3 and 20.1 kcal mol^{-1}, whereas relative energy of the disrot structure is 18.9 and 19.6 kcal mol^{-1} at CASSCF and MRMP2 levels, respectively. The computed geometries of MCP and MCP/$\mathbf{o}_1$ structures are shown in Figure 15, while geometries of the conrot and disrot structures are shown in Figure 16.

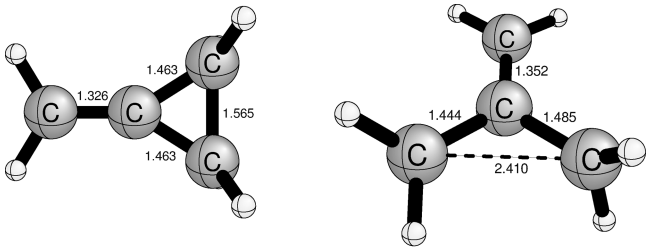

(a) **MCP** (b) **MCP/o$_1$**

Figure 15. Selected interatomic distances (Å) for the MCP and MCP/$\mathbf{o}_1$ structures.

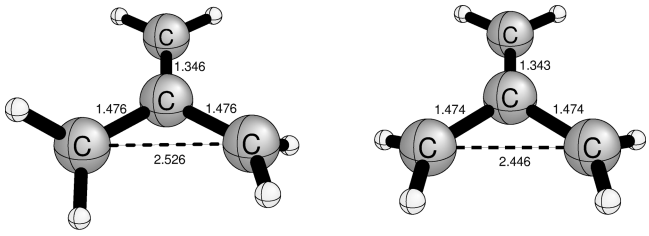

(a) ***conrot*** (b) ***disrot***

Figure 16. Selected interatomic distances (Å) for the *conrot* and *disrot* structures.

Berson-TMMa System. Qualitative structures of the Berson-TMMa stationary points are illustrated in Figure 17,

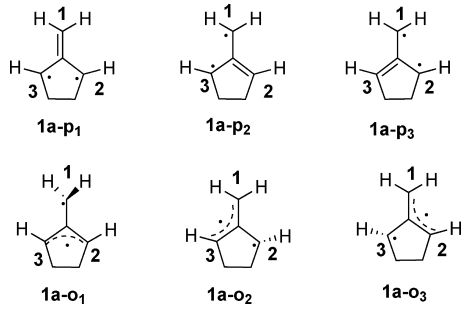

Figure 17. Structures in the Berson-TMMa system. Abbreviations: **p**, planar; **o**, orthogonal methylene group. In all structures, carbon atoms of methylene groups are labeled by 1, 2, and 3 clockwise, starting with the top methylene. The subscripts in $\mathbf{p}_n$ and $\mathbf{o}_n$ indicate position of the double bond or the orthogonal methylene.

while ZPVE-corrected relative energies are reported in Table 2. Four electronic states of the Berson-TMMa system, namely, $^3B_2$, $^1A_1$, $^1B_1$, and $^1B_2$ have been investigated. An active space of four electrons and four orbitals (4e,4o) have been used in the CASSCF and MRMP2 computations as in the case of the parent TMMs.

dx.doi.org/10.1021/jp211518f | J. Phys. Chem. A 2012, 116, 2309−2321

Table 2. ZPVE-Corrected Relative Energies (in kcal mol^{-1}) of the Berson-TMMa Structures with 6-311G(d,p) Basis Set

structure	(4e,4o)CASSCF	(4e,4o)MRMP2
triplet	0.0	0.0
1a-o$_1$	13.6	14.8
1a-o$_2$	17.5	17.8
1a-p$_1$	17.0	16.5
1a-p$_2$	17.8	18.2
1a-p-l$_1$	16.7	16.2

Triplet TMMa. Using the CASSCF method we found that triplet TMMa($^3B_2$) is a minimum on the potential energy surface at C_{2v} geometry. In order to construct a relative energy scale for the Berson-TMMa structures we used TMMa($^3B_2$) as a reference molecule and we set relative energy of the triplet to zero. Therefore, energies of other structures will be given relative to energy of TMMa($^3B_2$). The computed geometry of the TMMa($^3B_2$) structure is shown in Figure 18.

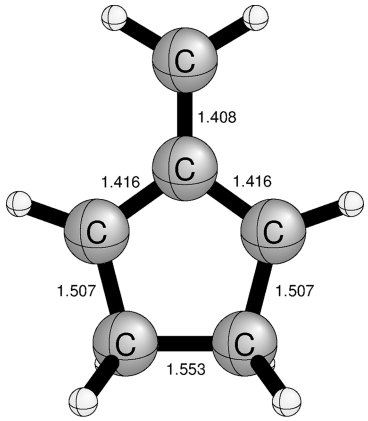

Figure 18. Selected interatomic distances (Å) for the triplet TMMa(C_{2v},$^3B_2$) structure.

Orthogonal TMMa. At the CASSCF level, the optimum geometry of the **1a-o$_1$**($^1B_1$) structure is a transition state. The imaginary frequency is 219.9i cm^{-1} and connects two equivalent pyramidalized structures with C_s symmetry. We found a minimum at C_s geometry with a slightly pyramidalized (10.0°) methylene group which includes the C_1 atom (see Figure 17 for numbering of the TMMa carbon atoms). The state symmetry of that C_s structure is A″. The **1a-o$_1$**(A″) structure is 0.4 kcal mol^{-1} lower in energy than **1a-o$_1$**($^1B_1$) at the CASSCF level, whereas at the MRMP2 level **1a-o$_1$**($^1B_1$) is 0.6 kcal mol^{-1} lower in energy than **1a-o$_1$**(A″). Therefore, we conclude that the pyramidalization is an artifact of the CASSCF method as in case of the parent TMM system. Relative energy of the **1a-o$_1$**(A″) structure is 13.6 and 14.8 kcal mol^{-1} at the CASSCF and MRMP2 levels, respectively.

It should be recalled that in the parent TMM system, the **o$_1$**−triplet energy splitting is 13.7 and 14.9 kcal mol^{-1} at the CASSCF and MRMP2 levels, respectively. Thus, in the TMMa system the computed lowest singlet−triplet splitting energies are almost the same as in the parent TMM system, the difference being only 0.1 kcal mol^{-1} at the CASSCF and MRMP2 levels. This fact indicates that the fundamental characteristic of the parent TMM PES is maintained in TMM derivatives, and substituents do not change the relative energies significantly.

Furthermore, we again found another slightly pyramidalized minimum structure corresponding to the **1a-o$_2$** structure at C_1 geometry. The relative energy of the **1a-o$_2$** structure is 17.5 and 17.8 kcal mol^{-1} at the CASSCF and MRMP2 levels, respectively. The relative energy of the **1a-o$_2$** structure is 3.9 and 3.0 kcal mol^{-1} higher than that of the **1a-o$_1$**(A″) structure at the CASSCF and MRMP2 levels, respectively, due to the ring strain. In orthogonal structures, one methylene group tends to be 90° rotated from the plane. However, in the **1a-o$_2$** structure the ring strain prevents a rotation of 90°. Therefore, the **1a-o$_2$** structure is higher in energy than **1a-o$_1$**. The computed geometries of the **1a-o$_1$**($^1B_1$), **1a-o$_1$**(A″), and **1a-o$_2$** structures are shown in Figure 19.

Planar TMMa. We found two stationary points corresponding to the **1a-p$_1$** structure. One of them is a transition state at C_{2v} geometry ($^1A_1$) with an imaginary frequency of 83.5i cm^{-1}, and the other is a minimum at C_2 geometry (^1A). The C_{2v} structure is 0.02 and 0.08 kcal mol^{-1} lower in energy than the C_2 structure at the CASSCF and MRMP2 levels, respectively. Relative energies of the **1a-p$_1$**($^1A_1$) and **1a-p$_1$**(^1A) structures are 17.0 and 16.9 kcal mol^{-1} at the CASSCF level, while the analogous results are 16.5 and 16.4 kcal mol^{-1} at MRMP2 level, respectively. The calculated relative energies of **1a-p$_1$**($^1A_1$) differ by only 0.2 and 1.5 kcal mol^{-1} from its corresponding analogue in the parent TMM system (**s$_1$**) at the CASSCF and MRMP2 levels, respectively. Again, it can be concluded that the major aspects of the parent TMM PES does not change significantly with substituent effects.

Furthermore, for the **1a-p$_2$** structure we only found a transition structure with an imaginary frequency of 440.3i cm^{-1} at C_1 geometry. The relative energy of **1a-p$_2$** is 17.8 and 18.2 kcal mol^{-1} at the CASSCF and MRMP2 levels, respectively. Since for the **1a-p$_2$** structure only a TS is found and for the **1a-p$_1$** structure the relative energy of the TS is lower than that of the minimum, we concluded that the planar structures are TSs. The computed geometries of the **1a-p$_1$**($^1A_1$), **1a-p$_1$**(^1A), and **1a-p$_2$** structures are shown in Figure 20.

Moreover, we calculated that the **1a-p-l$_1$**($^1B_2$) structure, which is the analogue of the **l$_1$** structure of the parent TMM, is a third-order saddle point. Corresponding imaginary frequencies are 573.5i, 366.4i, and 276.7i cm^{-1}. The vibrational mode corresponding to imaginary frequency 573.5i cm^{-1} connects the **1a-p$_2$** and **1a-p$_3$** structures by a reaction path which has C_1 symmetry. The vibrational mode corresponding to imaginary frequency 366.4i cm^{-1} connects two equivalent pyramidalized planar structures by a reaction path which has C_s symmetry. The mode corresponding to imaginary frequency 276.7i cm^{-1} connects two equivalent **1a-o$_1$** structures by a reaction path of C_2 symmetry. Relative energies of the **1a-p-l$_1$** structure are 16.7 and 16.2 kcal mol^{-1} at the CASSCF and MRMP2 levels, respectively. Again, the relative energy of the long planar structure (**1a-p-l$_1$**) is quite close to that of its corresponding analogue in the parent TMM system (**l$_1$**). Relative energies of **1a-p-l$_1$** differ by less than 0.5 kcal mol^{-1} from those of **l$_1$**. The computed geometry of the **1a-p-l$_1$** structure is shown in Figure 21.

Rearrangements Involving Berson-TMMa Structures. Rearrangements among **1a**, **3a**, **4a**, and **5a** have been investigated next. In analogy with their monocyclic counterparts, the bicyclic MCPs **3a** and **5a** are expected to ring open to TMMs by a single-step reaction path (Figure 22). This anticipation is born out by **5a**, which opens to **1a-o$_1$** with C_1 acting as pivot carbon. The computed barrier to the ring-

dx.doi.org/10.1021/jp211518f | J. Phys. Chem. A 2012, 116, 2309−2321

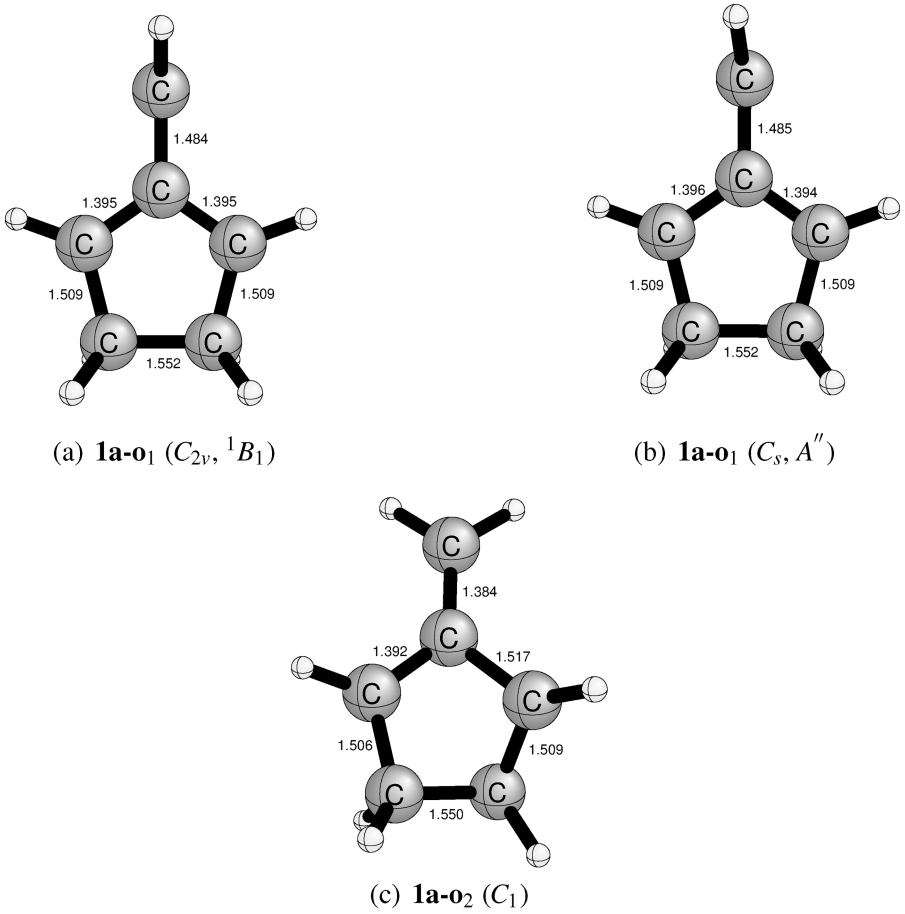

Figure 19. Selected interatomic distances (Å) for the **1a-o**$_1$(C_{2v},^{1}B$_1$), **1a-o**$_1$(C_s,A″), and **1a-o**$_2$(C_1) structures.

opening of **5a** is 23.7 − 5.2 = 18.5 kcal mol^{-1}, a value much smaller than 39.9 kcal mol^{-1} in the parent MCP. The lowering in the barrier is expected in view of the large strain in the double bond of **5a**, a point that will be discussed below. We were unable to locate a TS for the direct path connecting **5a** with **1a-o**$_2$ in which C$_2$ would be the pivot carbon. Further, the activation energy for conversion of **5a** to **3a** (**5a** → **3a**) is calculated as 18.5 kcal mol^{-1} (23.7 − 5.2 = 18.5), which is close to the predicted upper limit of 16.8 kcal mol^{-1} for a trimethyl substituted analogue.[9] The computed geometries of the **5a** and **1a**/**5a** structures are shown in Figure 23.

In the ring-opening of **3a**, the expected immediate product is **1a-o**$_2$. Unlike the nonsymmetric unique TS in the ring-opening of monocyclic MCP derivatives, we have located four stationary points on the path connecting **3a** with **1a-o**$_2$. Proceeding along the forward direction from **3a**, as in Figure 22, there is a TS with C_s symmetry, lying at 17.1 kcal mol^{-1} above **3a** at the MRMP2//CASSCF level. The TS mode (the vibration with the imaginary frequency) is totally symmetric and it leads to a second TS with C_{2v} symmetry. The TS mode in this second structure is a nontotally symmetric (b$_1$) vibration, and it lowers the symmetry to give the C_2 symmetric **1a-p**$_1$ species. At the CASSCF level, **1a-p**$_1$ is a minimum; however, when dynamical correlation (MRMP2) and ZPVE are included, its enthalpy moves slightly (0.1 kcal mol^{-1}) above that of the C_{2v} TS. The region of the PES involving these three structures is considerably flat, and it is very likely that the exact PES has no minima in these planar or nearly planar TMM regions. The fourth stationary point before reaching **1a-o**$_2$ is a TS with a geometry that qualitatively resembles the ring-opening TS in the parent TMM. It has the highest energy (17.4 kcal mol^{-1}) among the four, and therefore, the ring-opening barrier of **3a** to **1a-o**$_2$ is 16.4 kcal mol^{-1} at the MRMP2//CASSCF level, which is 2.6 kcal mol^{-1} lower than the barrier between **5a** and **1a-o**$_1$ at the same level. Furthermore, the computed barrier is in fair agreement with the experimental value of 13.7 kcal mol^{-1}.[7] The computed geometries of the **3a** and **1a**/**3a** structures are shown in Figure 24. The orthogonal TMM species **1a-o**$_2$ is a minimum. Admittedly, it is a shallow well, the barrier in the reverse direction to **1a-p**$_1$ from **1a-o**$_2$ being only 1.0 kcal mol^{-1}. Nevertheless, we believe that it is a true minimum.

Comparing to the parent TMM system, the activation energy for the ring-opening of **3a** to **1a-o**$_2$ is 23.5 kcal mol^{-1} lower than that for the MCP → **o**$_1$ reaction. The substantial lowering in the activation energy can be attributed to the high ring strain of **3a**. At the CCSD(T)//B3LYP level, the ring strain energy of **3a** is calculated as 27.5 kcal mol^{-1} relative to the strain energy of MCP via an isodesmic reaction[113] (Figure 25). Further, the computed strain energy for cyclobutane is 25.7 kcal mol^{-1} at the CCSD(T)//B3LYP level. Hence, our results show that the low barrier height of **3a** → **1a-o**$_2$ conversion can be traced to the high ring strain of the cyclobutane moiety in **3a**. A similar situation is also valid for the ring-opening of **5a** to **1a-o**$_1$, which is 21.4 kcal mol^{-1} lower than that for MCP. This small activation barrier may be attributed to the double bond strain in the five-membered ring. At the CCSD(T)//B3LYP level, the double bond strain energy of **5a** is calculated as 32.2 kcal mol^{-1} relative to that of MCP via an isodesmic reaction (Figure 26).

dx.doi.org/10.1021/jp211518f | J. Phys. Chem. A 2012, 116, 2309−2321

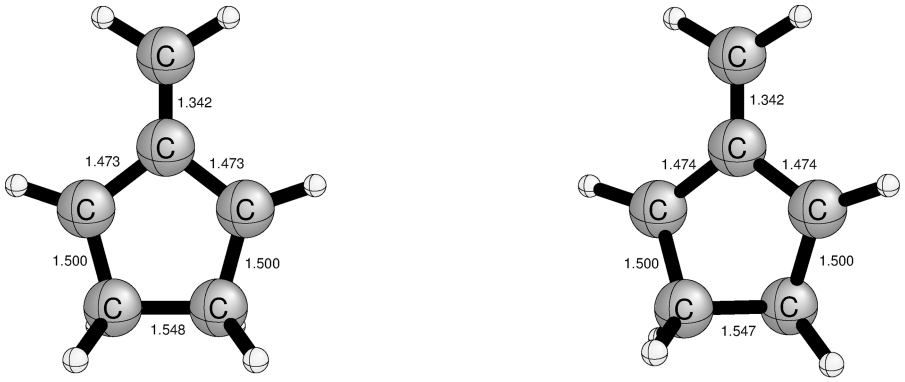

(a) **1a-p**$_1$ (C_{2v}, $^1A_1$) (b) **1a-p**$_1$ (C_2, ^1A)

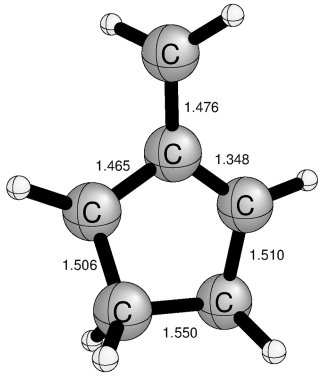

(c) **1a-p**$_2$ (C_1)

Figure 20. Selected interatomic distances (Å) for the **1a-p**$_1$(C_{2v},^{1}A$_1$), **1a-p**$_1$(C_2,^{1}A), and **1a-p**$_2$(C_1) structures.

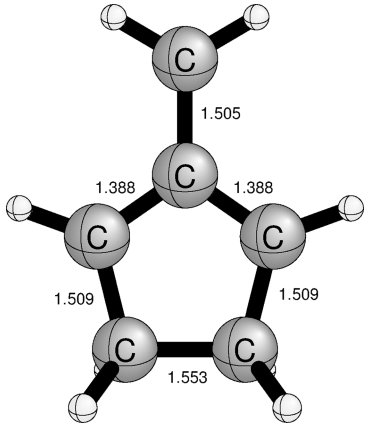

Figure 21. Selected interatomic distances (Å) for the **1a-p-l**$_1$(C_{2v},^{1}B$_2$) structure.

The computed strain energy is 10.8 kcal mol^{-1} higher than the activation energy barrier difference of 21.4 kcal mol^{-1} . The 10.8 kcal mol^{-1} difference is thought to be arising from somewhat stabilization of the double bond by alkyl groups in **5a**, since the more substituted alkenes (those with fewer hydrogens attached to the C=C) are more stable.[114]

The planar TMM species **1a-p**$_1$ can also rearrange to the lowest orthogonal TMM **1a-o**$_1$ with an enthalpy barrier of 18.3 − 16.5 = 1.8 kcal mol^{-1}. Additionally, it is involved in the 180° rotation of the methylene group in **1a-o**$_1$ about the C$_1$−C$_4$ bond and can play an important role in racemization of optically active, substituted **3a** or **5a**. The TS geometry (Figure 27) is similar to that of **1a-p**$_2$ (or **1a-p**$_3$).

The rearrangement of **1a-o**$_2$ to **4a** takes place via simultaneous bond breaking between C4−C5 carbon atoms and bond formation between C$_1$−C$_5$ and C$_3$−C$_4$ carbon atoms with a radical-involving mechanism. For this conversion, the reaction energy and barrier are computed as −39.1 and 15.7 kcal mol^{-1}, respectively. The computed geometries of **4a** and **1a**/**4a** are shown in Figure 28.

Rearrangements Involving Berson-TMMc Structures. Rearrangements among **1c**, **3c**, **4c**, **5c**, and **6c** have been investigated next (Figure 29). Relative energies differ by not more than 1−2 kcal mol^{-1} from those for the TMMa system. The computed geometries of the **5c** and **1c**/**5c** structures are shown in Figure 30, the **3c** and **1c**/**3c** structures in Figure 31, and the **4c** and **1c**/**4c** structures in Figure 32.

As distinct from the TMMa system, biradical **1c** can also rearrange to **6c** by 1,4-hydrogen shift. The reaction proceeds via a five-membered cyclic transition state (Figure 33). The calculated reaction energy and barrier are −58.0 and 15.2 kcal mol^{-1}, respectively. The **6c** molecule is thermodynamically the most stable isomer among the species involved in the TMMc system. Thus, in high temperature thermal reactions, the **6c** molecule should be expected as one of the major products, which is consistent with Berson et al.'s observation.[52] Computed geometries of the **6c** and **1c**/**6c** structures are shown in Figure 33.

dx.doi.org/10.1021/jp211518f | J. Phys. Chem. A 2012, 116, 2309−2321

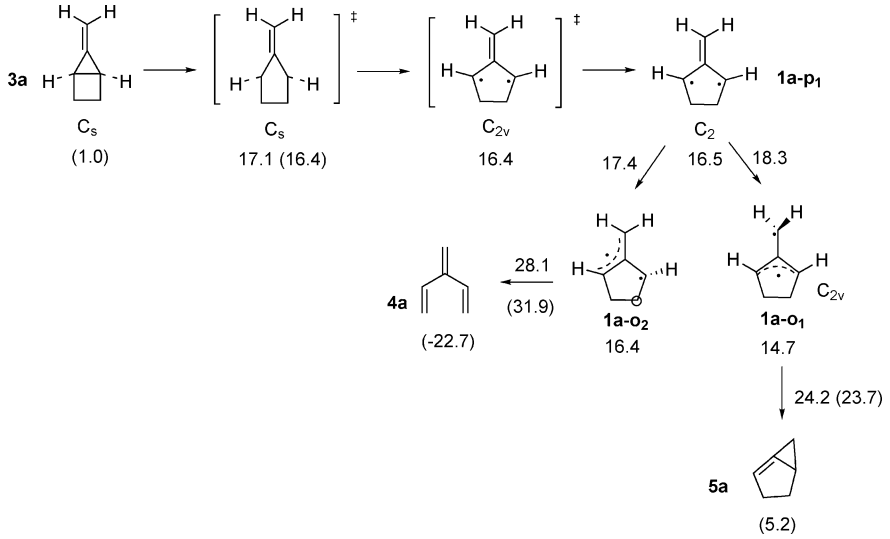

Figure 22. Reaction paths connecting the bicyclic MCPs, **3a**, **5a**, and species **4a**, with TMMs. ZPVE-corrected energies (in kcal mol^{-1}) relative to triplet TMMa at MRMP2//CASSCF and CCSD(T)//B3LYP (in parentheses) are indicated. A (4e,4o) active space is used except for the TS between **1a-o$_2$** and **4a**, where the active space employed is (6e,6o).

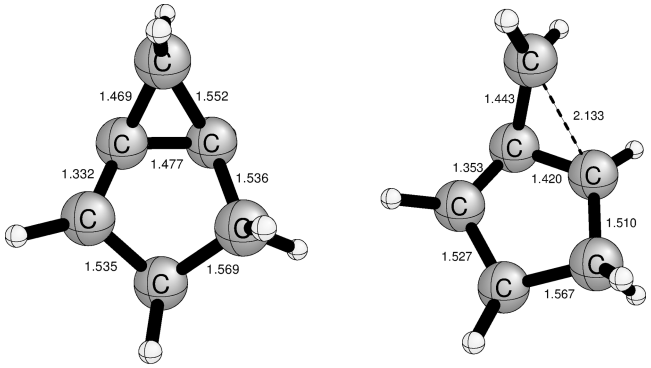

(a) **5a** (b) **1a/5a**

Figure 23. Selected interatomic distances (Å) for the **5a** and **1a**/**5a** structures.

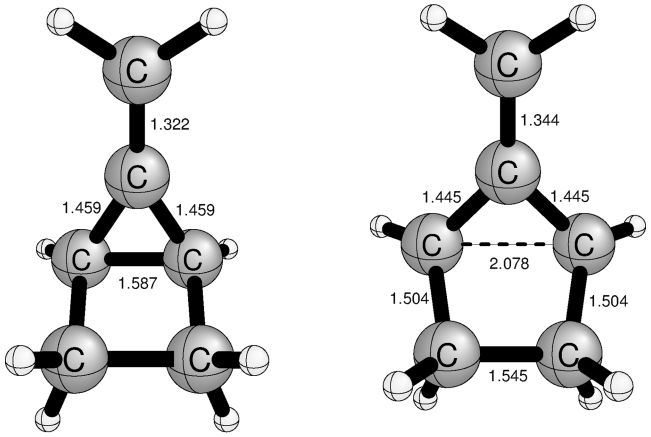

(a) **3a** (b) **1a/3a**

Figure 24. Selected interatomic distances (Å) for the **3a** and **1a**/**3a** (C_s symmetry) structures.

CONCLUSIONS

In this research, thermal rearrangements of Berson-TMMs and several other isomers connected to them by chemical reaction

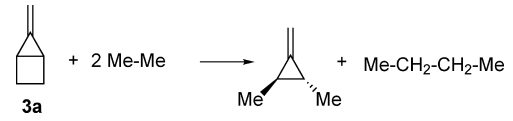

Figure 25. The isodesmic reaction for calculating the relative strain energy of **3a**.

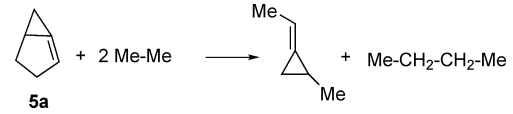

Figure 26. The isodesmic reaction for calculating the relative strain energy of **5a**.

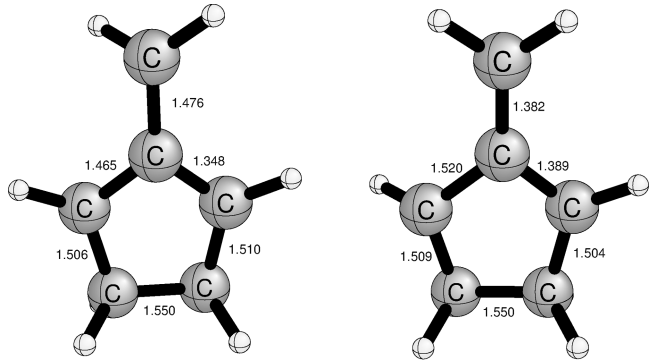

(a) **1a-p$_1$/1a-o$_1$** (b) **1a-p$_1$/1a-o$_2$**

Figure 27. Selected interatomic distances (Å) for the **1a-p$_1$**/**1a-o$_1$** and **1a-p$_1$**/**1a-o$_2$** structures.

pathways have been investigated by employing the highest level of theory available within our computational facilities. The relevant portions of the lowest-energy, singlet-spin potential energy surfaces of the C_4H_6 (TMM), C_6H_8 (TMMa), and C_8H_{12} (TMMc) chemical systems have been explored in order to determine the reaction energies and activation parameters accurately, with the ultimate objective of providing a theoretical account of experiments by Berson on TMMc. For this purpose,

dx.doi.org/10.1021/jp211518f | J. Phys. Chem. A 2012, 116, 2309–2321

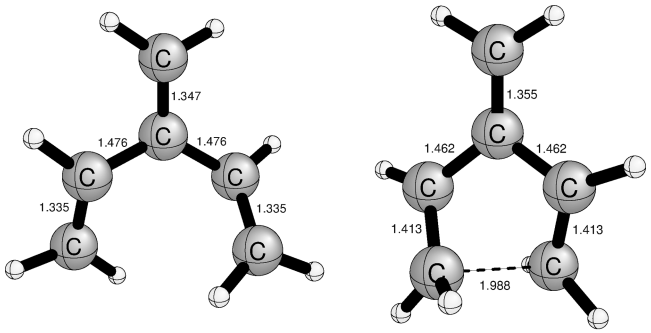

(a) **4a** (b) **1a/4a**

Figure 28. Selected interatomic distances (Å) for the **4a** and **1a**/**4a** structures.

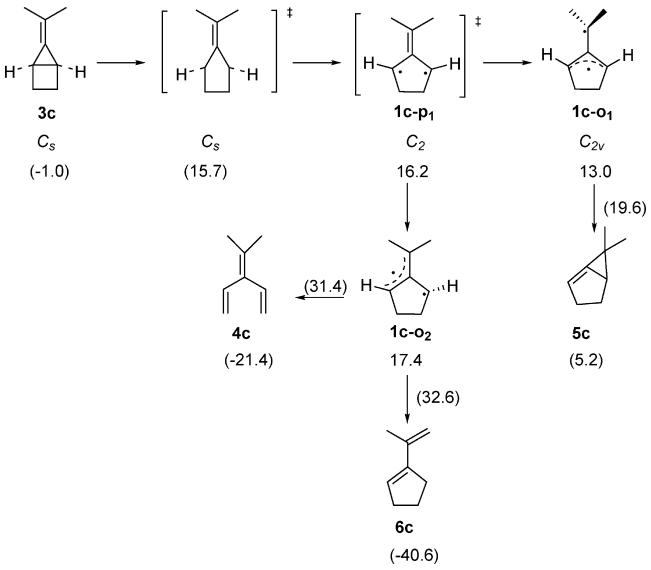

Figure 29. Reaction paths connecting the bicyclic MCPs, **3c**, **5c**, and species **4c** and **6c**, with TMMs. ZPVE-corrected energies (in kcal mol^{-1}) relative to triplet **1c-T** at MRMP2//CASSCF and CCSD(T)//B3LYP (in parentheses) are indicated. A (4e,4o) active space is used for biradicals.

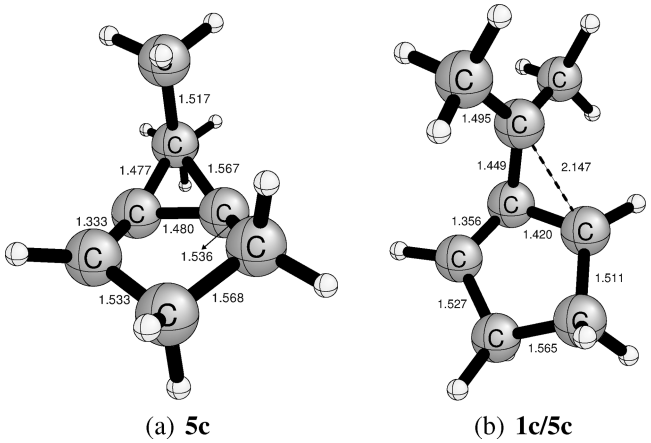

(a) **5c** (b) **1c/5c**

Figure 30. Selected interatomic distances (Å) for the **5c** and **1c**/**5c** structures.

a combination of DFT, CASSCF, MRMP2, MRCISD, and CCSD(T) methods have been employed, all with the triple-split valence 6-311G(d,p) basis set. Stationary points of closed-

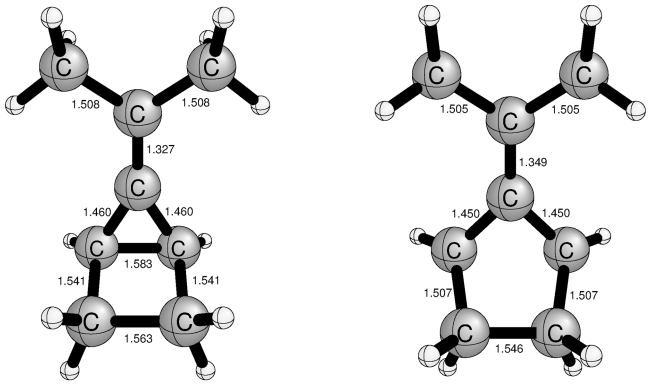

(a) **3c** (b) **1c/3c**

Figure 31. Selected interatomic distances (Å) for the **3c** and **1c**/**3c** structures.

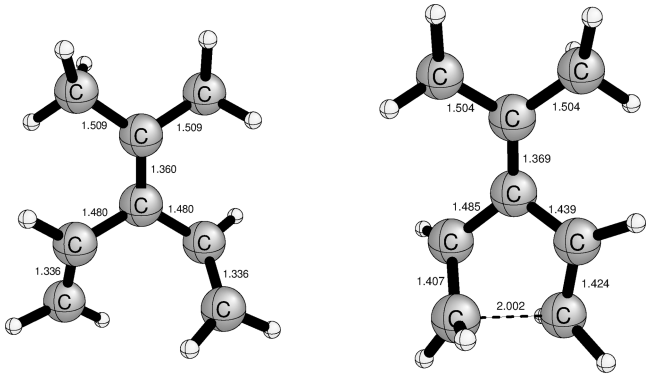

(a) **4c** (b) **1c/4c**

Figure 32. Selected interatomic distances (Å) for the **4c** and **1c**/**4c** structures.

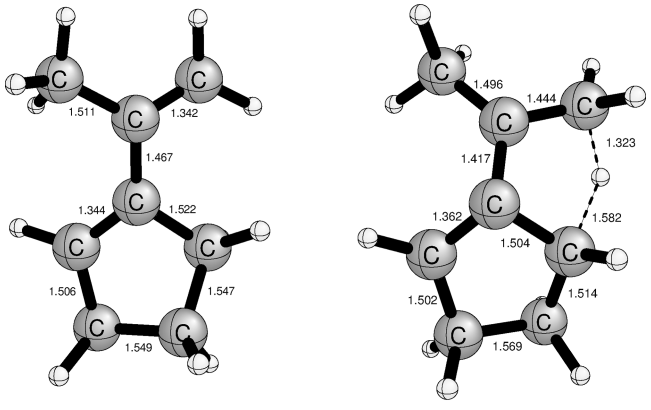

(a) **6c** (b) **1c/6c**

Figure 33. Selected interatomic distances (Å) for the **1c** and **1c**/**6c** structures.

shell species have been located at DFT and CASSCF levels, while only CASSCF has been used for the open-shell singlets (biradicals). Dynamical correlation is included by single-point CCSD(T) calculations for the former and by MRMP2 and MRCISD for the latter species. ZPVE corrections are at the DFT level for CCSD(T) relative energies, while at the CASSCF level for MRMP2 and MRCISD energies.

The nature of the orthogonal and the planar structures of the parent TMM have been clarified in this study. We have

dx.doi.org/10.1021/jp211518f | J. Phys. Chem. A 2012, 116, 2309–2321

concluded that the orthogonal TMM $^1B_1$ minimum has a C_{2v} symmetric structure, and there is no pyramidalization in the unique methylene group. It lies at 13.9 kcal mol^{-1} above the triplet minimum $^3B_2$ at the MRCISD level. The closed-shell $^1A_1$ state of the planar TMM is not a true minimum, but a TS for 180° rotation of the unique methylene group in the orthogonal TMM minimum. It lies at 3.0 kcal mol^{-1} above $^1B_1$. The planar structures are also involved in the interchange of equivalent orthogonal TMMs ($\mathbf{o}_1$, $\mathbf{o}_2$, $\mathbf{o}_3$). The activation energy from MCP has been calculated as 39.9 kcal mol^{-1}, in good agreement with the experimental value of 41.2 kcal mol^{-1} (LeFevre and Crawford[50]).

Many features of the parent TMM are retained in TMMa and TMMc, despite the constraints imposed by the five-membered ring in the latter species.[115] Thus ring-closure to the bicyclic molecules **3a** (**3c**) and **5a** (**5c**) takes place similarly to that in the parent TMM. Likewise, planar TMMa (TMMc) structures are TSs, while orthogonal ones are true minima. The adiabatic singlet−triplet gaps are also similar, being 14.7 (13.0) and 16.5 (16.2) kcal mol^{-1} in the orthogonal ($\mathbf{o}_1$) and planar TMMa (TMMc), respectively. It has been shown here that the substantial reductions in the ring-opening barriers of MCP derivatives **3a** (**3c**) and **5a** (**5c**) can be largely attributed to ring strain in the former and π-bond strain in the latter species.

■ ASSOCIATED CONTENT

Supporting Information

Cartesian coordinates, total energies, and ZPVE values for all stationary structures. This material is available free of charge via the Internet at http://pubs.acs.org.

■ AUTHOR INFORMATION

Corresponding Author

*E-mail: ugur.bozkaya@atauni.edu.tr (U.B.); ilker@metu.edu.tr (İ.Ö.).

Notes

The authors declare no competing financial interest.

■ ACKNOWLEDGMENTS

This research was supported by the Academic Staff Development Program, ÖYP-1624. U.B. thanks the Scientific and Technological Research Council of Turkey (TÜBİTAK) for supporting his scientific studies at the Middle East Technical University, BİDEB-2211.

■ REFERENCES

(1) Dewar, M. J. S. *The Molecular Orbital Theory of Organic Chemistry*; McGraw-Hill: New York, 1969; p 232.
(2) Berson, J. A. *Acc. Chem. Res.* **1997**, *30*, 238−244.
(3) Berson, J. A. *Angew. Chem., Int. Ed. Engl.* **1996**, *35*, 2750−2764.
(4) Gajewski, J. J. *Hydrocarbon Thermal Isomerizations*, 2nd ed.; Academic Press: New York, 2004; pp 41−46.
(5) Dowd, P. *Acc. Chem. Res.* **1972**, *5*, 242−248.
(6) Berson, J. A. *Acc. Chem. Res.* **1978**, *11*, 446−453.
(7) Mazur, M. R.; Berson, J. A. *J. Am. Chem. Soc.* **1982**, *104*, 2217−2222.
(8) Rule, M.; Mondo, J. A.; Berson, J. A. *J. Am. Chem. Soc.* **1982**, *104*, 2209−2216.
(9) Salinaro, R. F.; Berson, J. A. *J. Am. Chem. Soc.* **1982**, *104*, 2228−2232.
(10) Dowd, P. *J. Am. Chem. Soc.* **1966**, *88*, 2587−2589.
(11) Baseman, R. J.; Pratt, D. W.; Chow, M.; Dowd, P. *J. Am. Chem. Soc.* **1976**, *98*, 5726−5727.
(12) Dowd, P.; Chow, M. *J. Am. Chem. Soc.* **1977**, *99*, 2825−2827.
(13) Dowd, P.; Chow, M. *J. Am. Chem. Soc.* **1977**, *99*, 6438−6440.
(14) Dowd, P.; Chow, M. *Tetrahedron* **1982**, *38*, 799−807.
(15) Gajewski, J. J.; Paul, G. C. *J. Org. Chem.* **1997**, *62*, 7189−7191.
(16) Dolbier, W. R.; Burkholder, J. R. *J. Am. Chem. Soc.* **1984**, *106*, 2139−2142.
(17) Berson, J. A.; Turro, N. J.; Mircbach, M. J.; Harrit, N.; Platz, M. S. *J. Am. Chem. Soc.* **1978**, *100*, 7653−7658.
(18) Baum, T.; Rossi, A.; Srinivasan, R. *J. Am. Chem. Soc.* **1985**, *107*, 4411−4415.
(19) Leigh, W. J.; Srinivasan, R. *Acc. Chem. Res.* **1987**, *20*, 107−114.
(20) Wenthold, P. G.; Hu, J.; Squires, R. R.; Lineberger, W. C. *J. Am. Chem. Soc.* **1996**, *118*, 475−476.
(21) Wenthold, P. G.; Hu, J.; Squires, R. R.; Lineberger, W. C. *J. Am. Chem. Soc. Mass. Spec.* **1999**, *10*, 800−809.
(22) Wenthold, P. G.; Lineberger, W. C. *Acc. Chem. Res.* **1999**, *32*, 597−604.
(23) Schaefer, H. F.; Yarkony, D. R. *J. Am. Chem. Soc.* **1974**, *96*, 3754−3758.
(24) Goddard, W. A.; Davis, J. H. *J. Am. Chem. Soc.* **1976**, *98*, 303−304.
(25) Goddard, W. A.; Davis, J. H. *J. Am. Chem. Soc.* **1977**, *99*, 4242−4247.
(26) Dixon, D. A.; Foster, R.; Halgren, T. A.; Lipscomb, W. N. *J. Am. Chem. Soc.* **1978**, *100*, 1359−1365.
(27) Davidson, E. R.; Borden, W. T. *J. Am. Chem. Soc.* **1977**, *99*, 2053−2060.
(28) Davidson, E. R.; Borden, W. T. *J. Am. Chem. Soc.* **1977**, *99*, 4587−4594.
(29) Pitzer, R. M.; Hood, D. M.; Schaefer, H. F. *J. Am. Chem. Soc.* **1978**, *100*, 2227−2228.
(30) Pitzer, R. M.; Schaefer, H. F. *J. Am. Chem. Soc.* **1978**, *100*, 8009−8010.
(31) Dixon, D. A.; Dunning, T. H.; Eades, R. A.; Kleier, D. A. *J. Am. Chem. Soc.* **1981**, *103*, 2878−2880.
(32) Auster, S. B.; Pitzer, R. M.; Platz, M. S. *J. Am. Chem. Soc.* **1982**, *104*, 3812−3815.
(33) Feller, D.; Tanaka, K.; Davidson, E. R.; Borden, W. T. *J. Am. Chem. Soc.* **1982**, *104*, 967−972.
(34) Davidson, E. R.; Borden, W. T. *J. Phys. Chem.* **1983**, *87*, 4783−4790.
(35) Borden, W. T.; Du, P. *J. Am. Chem. Soc.* **1987**, *109*, 5330−5336.
(36) Skancke, A.; Schaad, L. J.; Hess, B. D. *J. Am. Chem. Soc.* **1988**, *110*, 5315−5316.
(37) Ma, B. Y.; Schaefer, H. F. *Chem. Phys.* **1996**, *207*, 31−41.
(38) Davidson, E. R.; Gajewski, J. J.; Shook, C. A.; Cohe, T. *J. Am. Chem. Soc.* **1995**, *117*, 8495−8501.
(39) Cramer, C. J.; Smith, B. A. *J. Phys. Chem.* **1996**, *100*, 9664−9670.
(40) Lijser, H. J. P. D; Arnold, D. R. *J. Phys. Chem.* **1996**, *100*, 3996−4010.
(41) Schaad, L. J.; Hu, J. *J. Am. Chem. Soc.* **1998**, *120*, 1571−1580.
(42) Borden, W. T.; Lewis, S. B.; Hrovat, D. A. *J. Chem. Soc., Perkin Trans.* **1999**, *2*, 2339−2347.
(43) Slipchenko, L. V.; Krylov, A. I. *J. Chem. Phys.* **2002**, *117*, 4694−4707.
(44) Slipchenko, L. V.; Krylov, A. I. *J. Chem. Phys.* **2003**, *118*, 6874−6883.
(45) Datta, S. N.; Mukherjee, P.; Jha, P. P. *J. Phys. Chem. A* **2003**, *107*, 5049−5057.
(46) Ikeda, H.; Namai, H.; Taki, H.; Miyashi, T. *J. Org. Chem.* **2005**, *70*, 3806−3813.
(47) Pittner, J.; Brabec, J. *J. Phys. Chem. A* **2006**, *110*, 11765−11769.
(48) Borden, W. T.; Lewis, S. B.; Hrovat, D. A. *J. Am. Chem. Soc.* **2006**, *128*, 16676−16683.
(49) Chesick, J. P. *J. Am. Chem. Soc.* **1963**, *85*, 2720−2723.
(50) LeFevre, G. N.; Crawford, R. J. *J. Org. Chem.* **1986**, *51*, 747−749.
(51) Jahn, H. A.; Teller, E. *Proc. R. Soc. London* **1937**, *A161*, 220−235.

(52) Mazur, M. R.; Potter, S. E.; Pinhas, A. R.; Berson, J. A. *J. Am. Chem. Soc.* **1982**, *104*, 6823−6824.
(53) Adam, W.; Finzel, R. *J. Am. Chem. Soc.* **1992**, *114*, 4563−4568.
(54) Paul, G. C.; Gajewski, J. J. *J. Org. Chem.* **1996**, *61*, 1399−1404.
(55) Kelley, D. F.; Rentzepis, P. M.; Mazur, M. R.; Berson, J. A. *J. Am. Chem. Soc.* **1982**, *104*, 3764−3766.
(56) Lazzara, M. G.; Harrison, J. J.; Rule, M.; Hilinski, E. F.; Berson, J. A. *J. Am. Chem. Soc.* **1982**, *104*, 2233−2243.
(57) Schmidt, S. P.; Pinhas, A. R.; Hammons, J. H.; Berson, J. A. *J. Am. Chem. Soc.* **1982**, *104*, 6822−6823.
(58) Salinaro, R. F.; Berson, J. A. *J. Am. Chem. Soc.* **1979**, *101*, 7094−7095.
(59) Rule, M.; Lazzara, M. G.; Berson, J. A. *J. Am. Chem. Soc.* **1979**, *101*, 7091−7092.
(60) Lazzara, M. G.; Harrison, J. J.; Rule, M.; Berson, J. A. *J. Am. Chem. Soc.* **1979**, *101*, 7092−7094.
(61) Osterman, V. M.; Schulte, G.; Berson, J. A. *J. Am. Chem. Soc.* **1989**, *111*, 8727−8729.
(62) Rule, M.; Salinaro, R. F.; Pratt, D. R.; Berson, J. A. *J. Am. Chem. Soc.* **1982**, *104*, 2223−2228.
(63) Borden, W. T.; Davidson, E. R. *Acc. Chem. Res.* **1981**, *14*, 69−76.
(64) Abe, M.; Kawanami, S.; Masuyama, A.; Hayashi, T. *J. Org. Chem.* **2006**, *71*, 6607−6610.
(65) Platz, M. S.; Berson, J. A. *J. Am. Chem. Soc.* **1977**, *99*, 5178−5180.
(66) Szabo, A.; Ostlund, N. S. *Modern Quantum Chemistry*; McGraw-Hill: New York, 1989; pp 258−260.
(67) Helgaker, T.; Jørgensen, P.; Olsen, J. *Molecular Electronic Structure Theory*; John Wiley & Sons: New York, 2000; pp 598−647.
(68) Shepard, R. *Adv. Chem. Phys.* **1987**, *69*, 63−200.
(69) Olsen, J.; Yeager, D. L.; Jørgensen, P. *Adv. Chem. Phys.* **1983**, *54*, 1−176.
(70) Roos, B. O. *Adv. Chem. Phys.* **1987**, *69*, 399−446.
(71) Shepard, R.; Shavitt, I.; Simons, J. *J. Chem. Phys.* **1982**, *76*, 543−557.
(72) Dalgaard, E.; Jørgensen, P. *J. Chem. Phys.* **1978**, *69*, 3833−3844.
(73) Dalgaard, E. *Chem. Phys. Lett.* **1979**, *65*, 559−563.
(74) Yeager, D. L.; Jørgensen, P. *J. Chem. Phys.* **1979**, *71*, 755−760.
(75) Werner, H.-J. *Adv. Chem. Phys.* **1987**, *69*, 1−62.
(76) Chaban, G.; Schmidt, M. W.; Gordon, M. S. *Theor. Chem. Acc.* **1997**, *97*, 88−95.
(77) Shepard, R. In *Modern Electronic Structure Theory*; 1st ed.; Advanced Series in Physical Chemistry Vol. 2; Yarkony, D. R., Ed.; World Scientific Publishing Co.: London, 1995; Part I, pp 345−458.
(78) Andersson, K.; Malmqvist, P.-A.; Roos, B. O.; Sadlej, A. J.; Wolinski, K. *J. Phys. Chem.* **1990**, *94*, 5483−5488.
(79) Andersson, K.; Malmqvist, P.-A.; Roos, B. O. *J. Chem. Phys.* **1992**, *96*, 1218−1226.
(80) Andersson, K.; Roos, B. O. In *Modern Electronic Structure Theory*; Advanced Series in Physical Chemistry Vol. 2; Yarkony, D. R., Ed.; World Scientific Publishing Co.: London, 1995; Part II, pp 55−109.
(81) Roos, B. O. In *Theory and Applications of Computational Chemistry: The First Forty Years*; Dykstra, C. E., Frenking, G., Kim, K. S., Scuseria, G., Eds.; Elsevier: Amsterdam, 2005; pp 725−764.
(82) Hirao, K. *Chem. Phys. Lett.* **1992**, *190*, 374−380.
(83) Hirao, K. *Chem. Phys. Lett.* **1992**, *196*, 397−403.
(84) Hirao, K. *Int. J. Quant. Chem. S.* **1992**, *26*, 517−526.
(85) Hirao, K. *Chem. Phys. Lett.* **1993**, *201*, 59−66.
(86) Sherrill, C. D.; Schaefer, H. F. In *Adv. Quantum Chem.*; Löwdin, P.-O., Ed.; Academic Press: New York, 1999; Vol. *34*, pp 143−269.
(87) Shavitt, I.; Bartlett, R. J. *Many-Body Methods in Chemistry and Physics*; Cambridge Press: New York, 2009; pp 185−250.
(88) Hoffmann, M. R. In *Modern Electronic Structure Theory*; Advanced Series in Physical Chemistry Vol. 2; Yarkony, D. R., Ed.; World Scientific Publishing Co.: London, 1995; Part II, pp 1166−1190.
(89) Purvis, G. D.; Bartlett, R. J. *J. Chem. Phys.* **1982**, *76*, 1910−1918.
(90) Pople, J. A.; Head-Gordon, M.; Raghavachari, K. *J. Chem. Phys.* **1987**, *87*, 5968−5975.
(91) Scuseria, G. E.; Scheiner, A. C.; Lee, T. J.; Rice, J. E.; Schaefer, H. F. *J. Chem. Phys.* **1987**, *86*, 2881−2890.
(92) Scuseria, G. E.; Janssen, C. L.; Schaefer, H. F. *J. Chem. Phys.* **1988**, *89*, 7382−7387.
(93) Crawford, T. D.; Schaefer, H. F. *Rev. Comp. Chem.* **2000**, *14*, 33−136.
(94) Bartlett, R. J. In *Modern Electronic Structure Theory*; Advanced Series in Physical Chemistry Vol. 2; Yarkony, D. R., Ed.; World Scientific Publishing Co.: London, 1995; Part II, pp 1047−1131.
(95) Bartlett, R. J.; Musial, M. *Rev. Mod. Phys.* **2007**, *79*, 291−352.
(96) Frisch, M. J.; Trucks, G. W.; Schlegel, H. B.; Scuseria, G. E.; Robb, M. A.; Cheeseman, J. R.; Montgomery, J. A.; Vreven, T.; Kudin, K. N.; Burant, J. C.; et al. *Gaussian 03, Revision D.01*; Gaussian, Inc.: Wallingford, CT, 2004.
(97) Schmidt, M. W.; Baldridge, K. K.; Boatz, J. A.; Elbert, S. T.; Gordon, M. S.; Jensen, J. H.; Koseki, S.; Matsunaga, N.; Nguyen, K. A.; Su, S. J.; Windus, T. L.; Dupuis, M.; Montgomery, J. A. *J. Comput. Chem.* **1993**, *14*, 1347−1363.
(98) cheMVP is free, open-source software designed to make clean, simple molecule drawings suitable for publications and presentations. The program is written in C++, using the QT library and some icons from the SVG icons project by A. Simmonett (andysim@ccc.uga.edu) and J. M. Turney (jturney@ccc.uga.edu), Center for Computational Quantum Chemistry (CCQC), University of Geoergia, 2008.
(99) Becke, A. D. *J. Chem. Phys.* **1993**, *98*, 5648−5652.
(100) Lee, C.; Yang, W.; Parr, R. G. *Phys. Rev. B* **1988**, *37*, 785−789.
(101) Ishida, K.; Morokuma, K.; Komornicki, A. *J. Chem. Phys.* **1977**, *66*, 2153−2156.
(102) Fukui, K. *Acc. Chem. Res.* **1981**, *14*, 363−368.
(103) Hratchian, H. P.; Schlegel, H. B. *J. Chem. Phys.* **2004**, *120*, 9918−9924.
(104) Hratchian, H. P.; Schlegel, H. B. In *Theory and Applications of Computational Chemistry: The First 40 Years*; Dykstra, C. E., Frenking, G., Kim, K. S., Scuseria, G., Eds.; Elsevier: Amsterdam, 2005; pp 195−249.
(105) Hratchian, H. P.; Schlegel, H. B. *J. Chem. Theory Comput.* **2005**, *1*, 61−69.
(106) Hariharan, P. C.; Pople, J. A. *Theor. Chem. Acc.* **1973**, *28*, 213−222.
(107) McLean, A. D.; Chandler, G. S. *J. Chem. Phys.* **1980**, *72*, 5639−5648.
(108) Krishnan, R.; Binkley, J. S.; Seeger, R.; Pople, J. A. *J. Chem. Phys.* **1980**, *72*, 650−654.
(109) Neumark, D. M. *Acc. Chem. Res.* **1993**, *26*, 33−39.
(110) Polanyi, J. C.; Zewail, A. H. *Acc. Chem. Res.* **1995**, *28*, 119−132.
(111) Gajewski, J. J. *J. Am. Chem. Soc.* **1968**, *90*, 7178−7179.
(112) Gajewski, J. J. *J. Am. Chem. Soc.* **1971**, *93*, 4450−4458.
(113) Jensen, F. *Introduction to Computational Chemistry*, 2nd ed.; John Wiley & Sons: New York, 1999; pp 221−222.
(114) Solomons, T. W. G.; Fryhle, C. B. *Organic Chemistry*, 10th ed.; John Wiley & Sons: New York, 2007; pp 288−291.
(115) Bozkaya, U. Ph.D. thesis, Middle East Technical University, Ankara, Turkey, 2011.